PHYSICAL REVIEW B VOLUME 45, NUMBER 13 1 APRIL 1992-I

Monte Carlo approach to the dynamical coherent-potential approximation in metallic magnetism

Y. Kakehashi
Department of Physics, Hokkaido Institute of Technology, Maeda, Teine-ku, Sapporo 006, Japan
(Received 15 August 1991)

A Monte Carlo approach to the dynamical coherent-potential approximation (CPA) has been proposed on the basis of the functional-integral method to deal with the dynamical spin fluctuations in the Gutzwiller-Hubbard model. The functional integral on a site in the effective medium is replaced by the N_ξ-fold integral, which is evaluated by the Monte Carlo method. Numerical calculations have been performed up to $N_\xi=64$ for intermediate Coulomb interaction strength in the paramagnetic state. It is demonstrated that the present theory recovers the amplitude of local moment, reduces the effective Coulomb interaction, and leads to more Fermi-liquid-like momentum distribution when they are compared with the static approximation. Furthermore, the single-particle excitation spectra calculated by a numerical analytic continuation are shown to have some shoulders due to many-body excitations.

I. INTRODUCTION

The theory of metallic magnetism has been extensively developed in the past decade.[1] The long-standing problem of the localized versus itinerant model in transition metals has been recognized to be solved by taking into account thermal spin fluctuations. The latter was formulated on the basis of the functional-integral method,[2,3] in which an interacting Hamiltonian is transformed into a one-electron system with time-dependent fictitious fields.

Cyrot[4] first adopted the method to the Gutzwiller-Hubbard model.[5,6] He showed that the method has an interpolation character between metal and insulator, which therefore indicated a possible explanation of the localized versus itinerant feature in transition metals. Hubbard[7] and Hasegawa[8] independently established the single-site spin fluctuation theory by making use of the coherent-potential approximation (CPA).[9] The theory has extensively been applied to various systems (e.g., crystals,[10,11] substitutional alloys,[12,13] surfaces,[14] liquids,[15] and amorphous systems[16]), and has explained qualitatively or semiquantitatively the magnetization versus temperature curves, the Curie temperatures (T_C), the Curie-Weiss susceptibilities, and large specific heats at T_C in transition metals and alloys.

Although many attempts to take into account more realistic band structure[17] or magnetic short-range order[18–20] have been made in the past decade, most of them are limited to the static approximation, which neglects the time dependence of fictitious fields. This approximation holds true at high temperatures, but causes some serious problems in the low-temperature regime.[11,12] In particular, the approximation reduces to the Hartree-Fock one at $T=0$. Thus it does not include the ground-state electron correlations as emphasized by Gutzwiller,[5] Hubbard,[6] and other investigators.[22] The local-electron correlations discussed by these investigators should persist even above T_C because associated correlation energies are much larger than T_C. Kakehashi and Fulde,[23,24] therefore developed a variational theory which adiabatically takes into account the Gutzwiller-type local-electron correlations.[25] The theory clarified that the electron correlations at finite temperatures reduce T_C (e.g., by a factor of 2 in the case of Fe),[24] strongly suppress the charge fluctuations even above T_C,[24] and greatly modify the thermal expansion coefficient.[26] A similar but more elegant theory has recently been developed by Hasegawa[27] on the basis of the slave-boson functional-integral technique.[28]

The theories mentioned above take into account the correlation energies adiabatically, but the entropy term remains unimproved. Moreover, the shortcomings in thermodynamics at low temperatures, which were found in the static approximation,[11,21] are not improved in the adiabatic approximation. Recently, Turov and Grebenikov[29] extended the single-site spin-fluctuation theory to the dynamical case. Hirooka and Shimizu[30] improved a variational theory by Hertz and Klenin,[31] optimizing an arbitrary parameter introduced in the functional-integral formalism. These theories are, however, limited to the small dynamical spin fluctuations.

On the other hand, various Monte Carlo methods[32–37] have recently been developed for quantum systems. In these approaches, the dynamical effects in a finite system are, in principle, exactly taken into account. Hirsch[34] developed the discrete Stratonovich-Hubbard transformation in which time-dependent field variables on each site take the discrete values ± 1. He performed a quantum Monte Carlo simulation for the narrow-band Gutzwiller-Hubbard model. His method is successful for one- and two-dimensional systems where one can take spatially large size of cluster. He also calculated the susceptibilities and energies for a three-dimensional simple-cubic $4\times4\times4$ cluster of the Gutzwiller-Hubbard model.[36] Calculated Néel temperatures T_N in the intermediate regime, which are 1.5 times higher than the results of our single-site variational theory, are, however, criticized to be overestimated by a factor of 2.[37] Although the Néel temperatures in the Monte Carlo method have been improved by extending the size of cluster up to $8\times8\times8$ (Ref. 38), they are considered still to be overestimated.[27] This is because the boundary condition is not necessarily

chosen so as to be best, in spite of the strong dependence of their results on it. In this respect, the traditional theories[7–18] in the metallic magnetism seem to be better than those in Monte Carlo approaches because they choose the best surrounding medium by using the CPA.

The aim of the present work is to improve a functional-integral theory of metallic magnetism by taking into account the merits in both approaches mentioned above; we propose the Monte Carlo dynamical CPA theory, in which the best medium is chosen by solving the CPA equation, while the single-site dynamical spin fluctuations are exactly taken into account by a Monte Carlo method. Such an improvement of the theory, we believe, should be a step towards a unified understanding of $3d$-, $4f$-, and $5f$- electron systems.[39]

The present paper is organized as follows. We formulate the dynamical CPA to the Gutzwiller-Hubbard model on the basis of the functional integral method in Sec. II. The difficulty which emerges after the formulation is how to perform the functional integrals along the imaginary time axis. We adopt the Monte Carlo technique to deal with this problem in Sec. III. In Sec. IV we present numerical examples for a model band with rectangular density of states (DOS). We will demonstrate by comparing the results with those in the static approximation how the dynamical effects improve the amplitude of local moment (LM), effective Coulomb interaction, momentum distribution, and the single-particle excitation spectrum. The last section will be devoted to a summary and discussions on possible improvements in the future.

II. DYNAMICAL CPA

The Hamiltonian which we consider here is the single-band Gutzwiller-Hubbard model[5,6] given by

$$\hat{H}=\sum_{i,\sigma}(\varepsilon_i^0-h_i\sigma)n_{i\sigma}+\sum_{i,j,\sigma}t_{ij}a_{i\sigma}^{\dagger}a_{j\sigma}+\sum_i U_0 n_{i\uparrow}n_{i\downarrow}\ . \tag{2.1}$$

Here ε_i^0 (h_i) is the atomic level (magnetic field) on site i, t_{ij} is the transfer integral between sites i and j, and U_0 is the on-site Coulomb interaction energy. $a_{i\sigma}^{\dagger}$ ($a_{i\sigma}$) denotes a creation (annihilation) operator on site i for an electron with spin σ, and $n_{i\sigma}=a_{i\sigma}^{\dagger}a_{i\sigma}$.

Since electrons satisfy the Pauli principle (i.e., $n_{i\sigma}^2=n_{i\sigma}$), the Hamiltonian (2.1) is rewritten as

$$\hat{H}=\sum_{i,\sigma}(\varepsilon_i^0+2\alpha U_0-h_i\sigma)n_{i\sigma}+\sum_{i,j,\sigma}t_{ij}a_{i\sigma}^{\dagger}a_{j\sigma}+\sum_i\tfrac{1}{4}(U_i n_i^2-J_i m_i^2)\ . \tag{2.2}$$

Here $U_i=(1-4\alpha)U_0$, $J_i=(1+4\alpha)U_0$, and α denotes an arbitrary c number.

We adopt the functional-integral method[2,3] to consider the finite-temperature problem. In this method, the interacting Hamiltonian (2.2) in the free energy is transformed into a one-electron Hamiltonian $H(\tau)$ with time-dependent random charge and exchange fields $\eta_i(\tau)$ and $\xi_i(\tau)$ on each site i. It is written in the interaction representation as follows:

$$H(\tau)=\sum_{i,\sigma}v_{i\sigma}(\tau)n_{i\sigma}(\tau)+\sum_{i,j,\sigma}t_{ij}a_{i\sigma}^{\dagger}(\tau)a_{j\sigma}(\tau)\ , \tag{2.3}$$

$$v_{i\sigma}(\tau)=\varepsilon_i^0-\mu-h_i\sigma+\tfrac{1}{2}[U_i i\eta_i(\tau)-J_i\xi_i(\tau)\sigma]\ . \tag{2.4}$$

Here μ is the chemical potential.

The free energy $\mathcal{F}$ is then given by

$$\mathcal{F}=-\beta^{-1}\ln\int\left[\prod_i\delta\xi_i\delta\eta_i\right]e^{-\beta E[\xi,\eta]}\ , \tag{2.5}$$

$$E[\xi,\eta]=-\beta^{-1}\ln Z_1[\xi,\eta]+\tfrac{1}{4}\sum_i\frac{1}{\beta}\int_0^{\beta}[U_i\eta_i(\tau)^2+J_i\xi_i(\tau)^2]d\tau\ , \tag{2.6}$$

$$Z_1[\xi,\eta]=\mathrm{Tr}\left[\mathcal{T}\exp\left[-\int_0^{\beta}H(\tau)d\tau\right]\right]\ . \tag{2.7}$$

Here β is the inverse temperature. $\mathcal{T}$ denotes the time-ordered product. The functional integral $\int\delta\xi_i$ in Eq. (2.5) is defined by

$$\int\delta\xi_i=\lim_{N'\to\infty}\int\left[\prod_{n=1}^{N'}\left[\frac{\beta J_i}{4\pi N'}\right]^{1/2}d\xi(\tau_n)\right]\ . \tag{2.8}$$

The integral $\int\delta\eta_i$ is defined in the same way, but J_i is replaced by U_i.

The partition function Z_1 in Eq. (2.6) is well-known to be expressed by the Green function as follows:[40]

$$\ln Z_1=\ln\mathrm{Tr}(e^{-\beta H_0})+\mathrm{Sp}(\ln g)+\mathrm{Sp}(\ln G^{-1})\ . \tag{2.9}$$

Here Sp denotes the trace with respect to site, time, and spin. The free-electron Hamiltonian H_0 and Green functions are defined as follows, respectively.

$$H_0=\sum_{i,j,\sigma}t_{ij}a_{i\sigma}^{\dagger}a_{j\sigma}\ , \tag{2.10}$$

$$(g)_{i\tau j\tau'\sigma}=g_{ij\sigma}(\tau-\tau')=-\frac{\mathrm{Tr}[e^{-\beta H_0}\mathcal{T}a_{i\sigma}(\tau)a_{j\sigma}^{\dagger}(\tau')]}{\mathrm{Tr}(e^{-\beta H_0})}\ , \tag{2.11}$$

$$(G)_{i\tau j\tau'\sigma}=G_{ij\sigma}(\tau,\tau')=-\frac{\mathrm{Tr}\left[\mathcal{T}a_{i\sigma}(\tau)a_{j\sigma}^{\dagger}(\tau')\exp\left[-\int_0^{\beta}H(\tau'')d\tau''\right]\right]}{\mathrm{Tr}\left[\exp\left[-\int_0^{\beta}H(\tau'')d\tau''\right]\right]}\ . \tag{2.12}$$

The Green function G satisfies the Dyson equation

$$G^{-1}=g^{-1}-v\ , \tag{2.13}$$

$$(v)_{i\tau j\tau'\sigma}=\Delta\tau v_{i\sigma}(\tau)\delta_{\tau\tau'}\delta_{ij}\ . \tag{2.14}$$

Here $\Delta\tau=\beta/N'$ is an infinitesimal fraction.

Next, we introduce the coherent potential $\Sigma_\sigma(\tau-\tau')$, which is independent of the fields $\xi_i(\tau)$ and $\eta_i(\tau)$, and rewrite $\mathrm{Sp}(\ln G^{-1})$ in Eq. (2.9) as follows:

$$\mathrm{Sp}(\ln G^{-1})=\mathrm{Sp}(\ln\tilde{G}^{-1})+\mathrm{Sp}\ln(1-\delta v\tilde{G}) , \tag{2.15}$$

$$\delta v=v-\Sigma . \tag{2.16}$$

Here the coherent Green function $\tilde{G}$ is defined by

$$\tilde{G}^{-1}=g^{-1}-\Sigma , \tag{2.17}$$

$$(\Sigma)_{i\tau j\tau'\sigma}=\Delta\tau\Sigma_\sigma(\tau-\tau')\Delta\tau\delta_{ij} . \tag{2.18}$$

Since we want to make a single-site approximation, we separate $\tilde{G}$ into the diagonal part F and the off-diagonal one F' with respect to site:

$$\tilde{G}=F+F' , \tag{2.19}$$

$$(F)_{i\tau j\tau'\sigma}=(\tilde{G})_{i\tau i\tau'\sigma}\delta_{ij} , \tag{2.20}$$

$$(F')_{i\tau j\tau'\sigma}=(\tilde{G})_{i\tau j\tau'\sigma}(1-\delta_{ij}) . \tag{2.21}$$

Substituting Eq. (2.19) into Eq. (2.15), we obtain the identity

$$\mathrm{Sp}(\ln G^{-1})=\mathrm{Sp}(\ln\tilde{G}^{-1})+\mathrm{Sp}\ln(1-\delta vF)+\mathrm{Sp}\ln[1-(1-\delta vF)^{-1}\delta vF'] . \tag{2.22}$$

Equations (2.9) and (2.22) lead to the following expansion of energy functional with respect to site:

$$E[\xi,\eta]=\tilde{\mathcal{F}}[\Sigma]+\sum_i E_i[\xi_i,\eta_i]+\Delta E[\xi,\eta] , \tag{2.23}$$

$$\tilde{\mathcal{F}}[\Sigma]=-\beta^{-1}[\ln\mathrm{Tr}(e^{-\beta H_0})+\mathrm{Sp}\ln(1-\Sigma g)] , \tag{2.24}$$

$$E_i[\xi_i,\eta_i]=-\beta^{-1}\mathrm{Sp}\ln(1-\delta v_iF_i)+\frac{1}{4\beta}\int_0^\beta d\tau[U_i\eta_i(\tau)^2+J_i\xi_i(\tau)^2] , \tag{2.25}$$

$$\Delta E[\xi,\eta]=-\beta^{-1}\mathrm{Sp}\ln(1-\tilde{t}F') , \tag{2.26}$$

$$\tilde{t}=(1-\delta vF)^{-1}\delta v . \tag{2.27}$$

Here $\tilde{\mathcal{F}}[\Sigma]$ is the free energy of the effective medium, $E_i[\xi_i,\eta_i]$ is the single-site energy functional, and $\Delta E[\xi,\eta]$ is the remaining term associated with the intersite electron correlations. We added suffix i to δv and F in Eq. (2.25) to indicate the matrix elements concerned with site i.

In the single-site approximation, we neglect $\Delta E[\xi,\eta]$ in Eq. (2.23). The free energy is then expressed as follows:

$$\mathcal{F}_{\mathrm{CPA}}=\tilde{\mathcal{F}}-\sum_i\beta^{-1}\ln\int\delta\xi_i\delta\eta_i e^{-\beta E_i[\xi_i,\eta_i]} . \tag{2.28}$$

The coherent potential Σ is determined so that the thermal average of the single-site t matrix (2.27) vanishes:

$$\langle\tilde{t}_i\rangle=-\frac{\int\delta\xi_i\delta\eta_i\tilde{t}_i e^{-\beta E_i[\xi_i,\eta_i]}}{\int\delta\xi_i\delta\eta_i e^{-\beta E_i[\xi_i,\eta_i]}}=0 . \tag{2.29}$$

This is called the CPA equation[9] and guarantees a real solution $\Sigma_\sigma(\tau-\tau')$. It should be noted that the CPA equation (2.29) leads to the stationary condition of the free energy,

$$\frac{\delta\mathcal{F}_{\mathrm{CPA}}}{\delta(\Sigma)_{i\tau i\tau'\sigma}}=0 . \tag{2.30}$$

Charge and local moment on site i is obtained from the free energy by taking the derivatives $\partial\mathcal{F}_{\mathrm{CPA}}/\partial\varepsilon_i^0$ and $-\partial\mathcal{F}_{\mathrm{CPA}}/\partial h_i$:

$$\langle n_i\rangle=\sum_\sigma F_{i\sigma}(-0) , \tag{2.31}$$

$$\langle m_i\rangle=\sum_\sigma\sigma F_{i\sigma}(-0) . \tag{2.32}$$

Here we used Eqs. (2.29) and (2.30). The above expression is quite adequate because the coherent Green function $F_{i\sigma}(\tau)$ is identical with the temperature Green function in the single-site approximation (see Appendix A).

We note that there exist alternative expressions of $\langle n_i\rangle$ and $\langle m_i\rangle$ with use of field variables (see Appendix B).

$$\langle n_i\rangle=\frac{1}{\beta}\int_0^\beta d\tau\langle -i\eta_i(\tau)\rangle , \tag{2.33}$$

$$\langle m_i\rangle=\frac{1}{\beta}\int_0^\beta d\tau\langle\xi_i(\tau)\rangle . \tag{2.34}$$

Here $\langle\ \rangle$ at the right-hand side denotes a thermal average with respect to $E_i[\xi_i,\eta_i]$ in the sense of Eq. (2.29).

The thermal averages of the squares of the local charge and local moment are obtained from $4\partial\mathcal{F}_{\mathrm{CPA}}/\partial U_i$ and $-4\partial\mathcal{F}_{\mathrm{CPA}}/\partial J_i$ as follows (see Appendix C):

$$\langle n_i^2\rangle=-\frac{1}{\beta}\int_0^\beta d\tau\langle\eta_i(\tau)^2\rangle+\frac{2}{U_i\Delta\tau} , \tag{2.35}$$

$$\langle m_i^2\rangle=\frac{1}{\beta}\int_0^\beta d\tau\langle\xi_i(\tau)^2\rangle-\frac{2}{J_i\Delta\tau} . \tag{2.36}$$

III. MONTE CARLO EVALUATION OF THE FUNCTIONAL INTEGRALS

In the following we consider the one-field case ($\alpha=\frac{1}{4}$),[40] and omit the site index i for brevity. It is more convenient for the purpose of numerical calculations to discretize the imaginary time (τ) into L segments with the same length $\Delta\tau=\beta/L$. The size of the matrices (Σ, g, v, F, and $\tilde{t}$) becomes then $L\times L$ with respect to the time. Since the coherent Green function satisfies the translational symmetry for imaginary time, it is diagonalized by the Fourier transform as follows:

$$F_\sigma(\tau-\tau')=\frac{1}{\beta}\sum_l F_\sigma(i\omega_l)e^{-i\omega_l(\tau-\tau')} , \tag{3.1}$$

$$F_\sigma(i\omega_l)=\int\frac{\hat{\rho}(\varepsilon)d\varepsilon}{g(\varepsilon,i\omega_l)^{-1}-\Sigma_\sigma(i\omega_l)} . \tag{3.2}$$

Here $\omega_l=(2l+1)\pi/\beta$, l being an integer such that $-L/2+1\le 2l+1\le L/2$. $\hat{\rho}(\varepsilon)$ in Eq. (3.2) denotes the DOS for the noninteracting Hamiltonian (2.10). $g(\varepsilon,i\omega_l)$ and $\Sigma_\sigma(i\omega_l)$ are the Fourier transforms of the free-electron Green function and the coherent potential,

which are defined by

$$g(\varepsilon,i\omega_l)=\frac{\Delta\tau}{1-e^{-(i\omega_l-\varepsilon)\Delta\tau}}\ , \tag{3.3}$$

$$\Sigma_\sigma(i\omega_l)=\sum_{n=1}^{L/2}\Sigma_\sigma(\tau_n)e^{i\omega_l\tau_n}\Delta\tau\ , \tag{3.4}$$

where $\tau_n=n\Delta\tau$.

The most difficult problem in the dynamical CPA described in the previous section is the evaluation of the functional integrals in the CPA equation (2.29) and other equations (2.33)–(2.36). Cyrot,[4] Sakoh and Shimizu,[41] Hubbard,[5] and Hasegawa[6] adopted the static approximation. It is reasonable at high temperatures since the range of imaginary time is small there. Turov and Grebenikov[29] expanded the energy functional with respect to the field variables, and evaluated the functional integrals by means of the Gaussian integrals. The approximation is valid for the weak electron-electron interaction regime.

We adopt the Monte Carlo approach to this problem. We replace the functional integral with the N_ξ-fold integrals, so that the average t matrix, for example, is expressed as follows:

$$\langle(\tilde{t})_{\tau_1\tau_2\sigma}\rangle=\frac{\int\left[\prod_{n=1}^{N_\xi}d\xi(\tau_n')\right](\tilde{t})_{\tau_1\tau_2\sigma}\det(1-\delta vF)\exp\left[-\frac{U_0\Delta\tau'}{2\beta}\sum_{n=1}^{N_\xi}\xi(\tau_n')^2\right]}{\int\left[\prod_{n=1}^{N_\xi}d\xi(\tau_n')\right]\det(1-\delta vF)\exp\left[-\frac{U_0\Delta\tau'}{2\beta}\sum_{n=1}^{N_\xi}\xi(\tau_n')^2\right]}\ . \tag{3.5}$$

Here $\Delta\tau'=\beta/N_\xi$ and $\tau_n'=n\Delta\tau'$. It should be noted that the fraction $\Delta\tau'$ is taken independently of $\Delta\tau=\beta/L$ for the size of matrices. Among various sampling techniques[32] for the Monte Carlo method, we adopted the simplest Gaussian sampling with the standard deviation $(\beta/U_0\Delta\tau')^{1/2}$.

The self-consistent solutions for $\varepsilon^0-\mu$ and $\{\Sigma_\sigma(\tau_n)\}$ are obtained as follows. First, we assume the inputs to be $(\varepsilon^0-\mu)_{\rm in}$ and $\Sigma_\sigma(\tau_n)_{\rm in}$ (for example, the Hartree-Fock values). Next, we derive $(\varepsilon^0-\mu)_{\rm out}$ [or $\Sigma_\sigma(0)_{\rm in}$] solving the charge neutrality condition (2.31). Generating the Gaussian random variables by means of the polar method, we calculate $(\tilde{t})_{\tau_n 0\sigma}$ solving the $L\times L$ simultaneous linear equations at each Monte Carlo step (MCS). When the CPA equations $\langle(\tilde{t})_{\tau_n 0\sigma}\rangle=0$ $(n=0,1,\ldots,L-1)$ are not satisfied after the Monte Carlo evaluation, we produce a new medium $\Sigma_\sigma(\tau_n)_{\rm out}$ according to the following relation:[9]

$$\Sigma_\sigma(\tau_n)_{\rm out}=\Sigma_\sigma(\tau_n)_{\rm in}+\left[(1+\langle\tilde{t}\rangle F)^{-1}\frac{\langle\tilde{t}\rangle}{(\Delta\tau)^2}\right]_{\tau_n 0\sigma}\ . \tag{3.6}$$

This procedure is continued until both charge-neutrality and CPA conditions are satisfied. Finally various quantities such as $\langle m\rangle$ and $\langle m^2\rangle$ are calculated by using the Monte Carlo samplings.

In this calculation, the case $N_\xi=1$ is identical with the one-field static approximation. When N_ξ is increased, the dynamical effects are taken into account. The single-site dynamical charge and spin fluctuations are exactly described in the limit $N_\xi\to\infty$ irrespective of the Coulomb interaction strength.

IV. NUMERICAL EXAMPLE

We have performed the numerical calculation to examine the reliability of our Monte Carlo approach to the dynamical CPA. The input DOS [$\hat{\rho}(\varepsilon)$ in Eq. (3.2)] is assumed to be rectangular with the atomic level $\varepsilon^0=0$ and the band width W. The Fourier transform of the coherent Green function is then given by

$$F_\sigma(i\omega_l)=\frac{\Delta\tau}{1-\Sigma_\sigma(i\omega_l)\Delta\tau}\left[1-\frac{1}{W\Delta\tau}\ln\frac{e^{i\omega_l\Delta\tau}[1-\Sigma_\sigma(i\omega_l)\Delta\tau]-e^{W\Delta\tau/2}}{e^{i\omega_l\Delta\tau}[1-\Sigma_\sigma(i\omega_l)\Delta\tau]-e^{-W\Delta\tau/2}}\right]\ . \tag{4.1}$$

We chose the parameters to be $W=0.5$ Ry and $U_0=0.2$ Ry bearing in mind transition metals. Needless to say, the accuracy and the temperature range inevitably depend on the efficiency and capacity of computers. We have fixed the size of matrices to be 1024×1024 (i.e., $L=1024$) in the HITAC S820/80 computer, and have continued the sampling up to 8000 MCS in maximum for each iteration obtaining the self-consistent coherent potential. We confine our results to the paramagnetic state in the present paper.

Figure 1 shows an example of calculated coherent potential for the electron number $n=1.5$. The static approximation produces a smooth negative curve in the interval $[0,\beta]$, except at $\tau/\beta=0$ where δ-function-like singularity proportional to $1/\Delta\tau$ takes place because of the static potential $\varepsilon^0-\mu$. When the dynamical effects are taken into account the coherent potential shows a rapidly oscillating structure, indicating an importance of the high-frequency components in the Fourier transform $\{\Sigma_\sigma(i\omega_l)\}$. In spite of a drastic change of $\Sigma_\sigma(\tau)$ due to

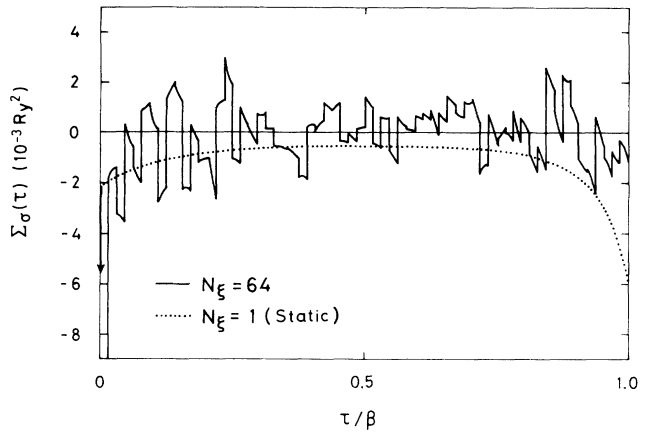

FIG. 1. Calculated self-energies for the electron number $n=1.5$, bandwidth $W=0.5$ Ry, and $U_0=0.2$ Ry at 2000 K. The dynamical result for $N_\xi=64$ variables and 8000 Monte Carlo steps (MCS) is shown by the solid curve, while the static case ($N_\xi=1$) for 4000 MCS is shown by the dotted curve. The arrow at $\tau/\beta=0$ indicates the δ-function-like singularity.

the dynamical effects, the coherent Green function $F_\sigma(\tau)$ is rather insensitive to N_ξ as shown in Fig. 2. The dynamical effects slightly increase the Green function in the short-time region ($0<\tau/\beta<0.10$), and decrease it in the remaining region ($0.10<\tau/\beta<1$). The effects, however, cause a serious change of structure in the single-particle excitation spectra, as will be shown later.

The most important question in the present approach is how many variables N_ξ one needs to describe dynamical effects. Numerical results for the amplitude of the LM in Fig. 3 give a rather optimistic answer to this question. The Monte Carlo result for $N_\xi=1$ is in agreement with the result of the static approximation obtained by an analytic method,[10] within a statistical error. When we increase N_ξ, the amplitude of the LM rapidly approaches the zone between the Hartree-Fock and LM limits. Although the accuracy is not enough to discuss the quantitative aspect because of a small number of samplings, we may conclude that the quantum effect on the amplitude

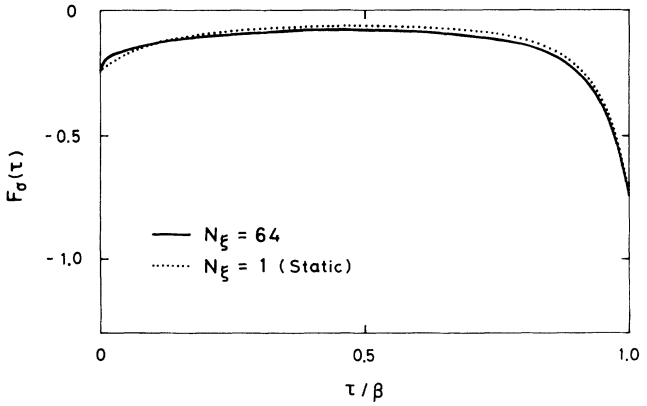

FIG. 2. Calculated coherent Green function with (——) and without (· · · ·) dynamical effects. Parameters are the same as in Fig. 1.

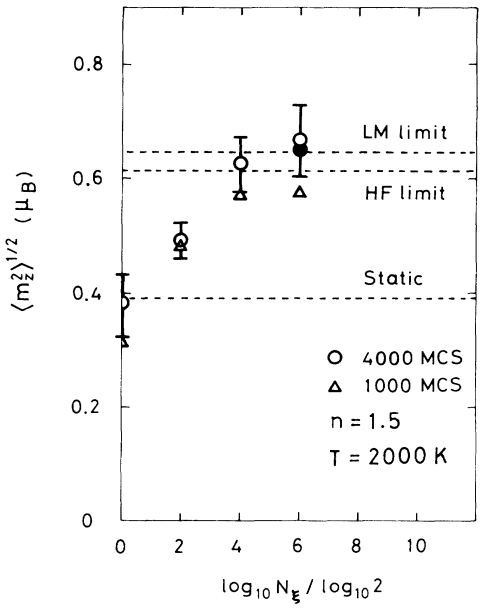

FIG. 3. Calculated amplitude of local moment (LM) as a function of the number of variables N_ξ. The closed circle at $N_\xi=64$ shows the result for 8000 MCS. Dashed lines show the results of the LM limit, Hartree-Fock limit, and the static approximation, respectively.

of the LM in the paramagnetic states with the intermediate Coulomb-interaction strength is described by taking into account the variables $N_\xi \gtrsim 50$.

Figure 4 shows the temperature change of the amplitude in both the static and dynamical cases. Our results indicate that the static approximation recovers the validity above 10 000 K, which is much higher than the Curie

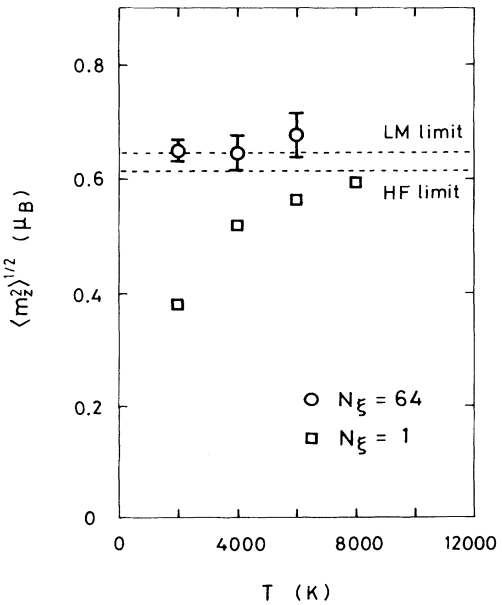

FIG. 4. Temperature dependence of the amplitudes of LM with (○: $N_\xi=64$, 8000 MCS) and without (□: $N_\xi=1$, 4000 MCS) dynamical effects in the case of $n=1.5$, $W=0.5$ Ry, and $U_0=0.2$ Ry.

temperatures (~ 100 K). On the other hand the dynamical results give the amplitudes close to the LM limit, although the accuracy is not enough for a quantitative evaluation. For a fixed number N_ξ, we need larger L (the size of matrices) for lower temperatures in the present approach since the upper limit of the imaginary time is equal to the inverse temperature β, and therefore requires more memory in a computer. On the other hand, we need more Monte Carlo steps for higher temperatures since the standard deviation in Gaussian sampling is in proportion to the temperature [see Eq. (3.5)] so that the range of sampling is extended.

Since the static approximation in the one-field method gives an exchange splitting twice as large as the Hartree-Fock one at low temperatures,[40] the dynamical effects should reduce it by more than a factor of 2. This feature manifests itself in the probability distribution function $P_{\rm eff}(\xi)$ [or the effective potential $E_{\rm eff}(\xi)$] projected onto the static field variable $\xi=\beta^{-1}\int_0^\beta \xi(\tau)d\tau$, which is defined by

$$P_{\rm eff}(\xi)=\frac{e^{-\beta E_{\rm eff}(\xi)}}{\int d\xi\, e^{-\beta E_{\rm eff}(\xi)}} =\frac{\int \delta\xi\,\delta\left[\xi-\beta^{-1}\int_0^\beta \xi(\tau)d\tau\right]e^{-\beta E[\xi]}}{\int \delta\xi\, e^{-\beta E[\xi]}}, \quad (4.2)$$

and is connected with the local magnetization $\langle m\rangle$ as follows [see Eq. (2.34)]:

$$\langle m\rangle=\int \xi P_{\rm eff}(\xi)d\xi\ . \quad (4.3)$$

We have calculated $P_{\rm eff}(\xi)$ by means of the Monte Carlo method, discretizing the functional integral in Eq. (4.2). Figure 5 shows the results for the electron number $n=1.5$. The Monte Carlo method reproduces the curve for the static approximation semiquantitatively. The distribution for $N_\xi=64$ slightly shrinks as compared with the static approximation ($N_\xi=1$), showing a reduction of the effective Coulomb interaction. This feature is more clearly seen in the case of $n=1.0$, as shown in Fig. 6. The local-moment behavior in the static approximation is strongly suppressed by the dynamical effects so that the distribution shows a single peak. If we fit the curve of $N_\xi=1$ to the dynamical result ($N_\xi=64$) changing the Coulomb interaction U_0, we obtain an effective Coulomb interaction $U_{\rm eff}$ between $0.4U_0$ and $0.5U_0$. This value is comparable to $U_{\rm eff}=0.45U_0$ obtained from the Gutzwiller-type energy functional.[37]

Overestimated random exchange fields in the static approximation are expected to spread excessively the momentum distributions $\langle n_{k\sigma}\rangle$. We therefore calculated $\langle n_{k\sigma}\rangle$ by using a formula

$$\langle n_{k\sigma}\rangle=\tilde{G}_{k\sigma}(-0) =\frac{1}{\beta}\sum_l [g(\varepsilon_k,i\omega_l)^{-1}-\Sigma_\sigma(i\omega_l)]^{-1}\ . \quad (4.4)$$

Here $\tilde{G}_{k\sigma}(\tau-\tau')$ denotes the momentum representation of the coherent Green function (2.19). $\{\varepsilon_k\}$ in Eq. (4.4) are the energy eigenvalues of the matrix t_{ij}, for which we have assumed a spherical-band model

$$\varepsilon_k=W\left[\left[\frac{k}{k_{\rm BZ}}\right]^3-\frac{1}{2}\right]. \quad (4.5)$$

Here $k_{\rm BZ}=(6\pi^2/\Omega)^{1/3}$, Ω being the volume per atom.

A numerical example of the momentum distribution for $n=1.0$ is presented in Fig. 7. We find more Fermi-liquid-like distributions when N_ξ is increased.

Finally, we discuss the single-particle excitation spectrum $\rho_\sigma(\omega)$. It is connected with the imaginary-time coherent Green function via the relation

$$F_\sigma(\tau)=-\int d\omega\,\rho_\sigma(\omega)\frac{e^{-\tau\omega}}{1+e^{-\beta\omega}}\ . \quad (4.6)$$

We adopted a method of numerical analytic continuation proposed by White, Sugar, Scalapino, and Bickers[42] to obtain the spectrum $\rho_\sigma(\omega)$ from the coherent Green function $F_\sigma(\tau)$. In this method, we use a modified least-

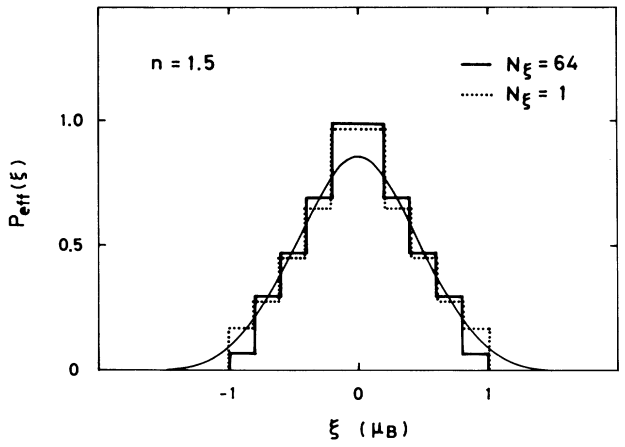

FIG. 5. Probability distribution function projected onto the static field variable $\xi=\beta^{-1}\int_0^\beta \xi(\tau)d\tau$. The thin curve is the result of the static approximation calculated from the analytic theory by Hasegawa (Ref. 8). The same parameters as in Fig. 1 are adopted.

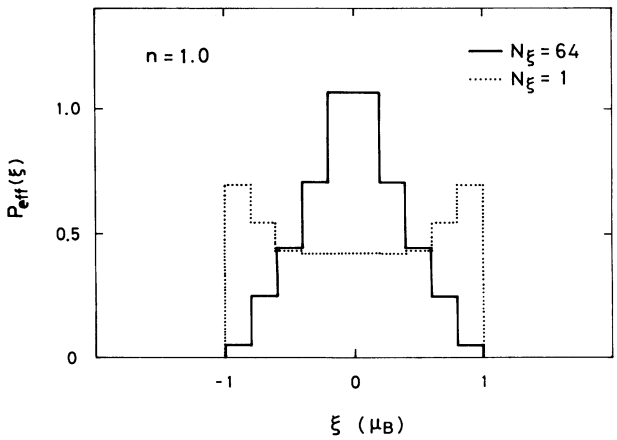

FIG. 6. The same as in Fig. 3 but for $n=1.0$ (half-filled case).

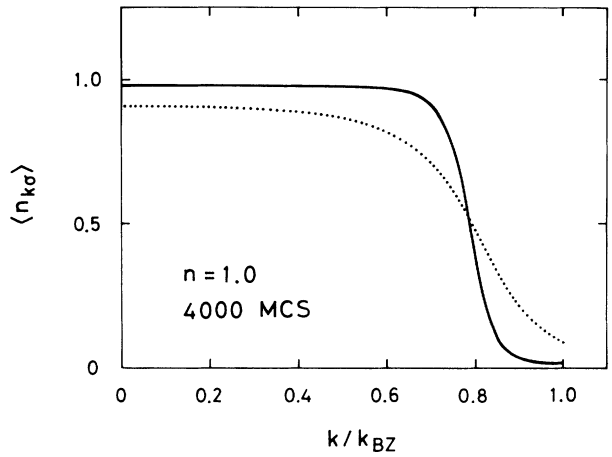

FIG. 7. Momentum distribution with (——: $N=64$) and without ($\cdots$: $N_\xi=1$) dynamical effect for $n=1.0$, $W=0.5$ Ry, $U_0=0.2$ Ry, and $T=4000$ K.

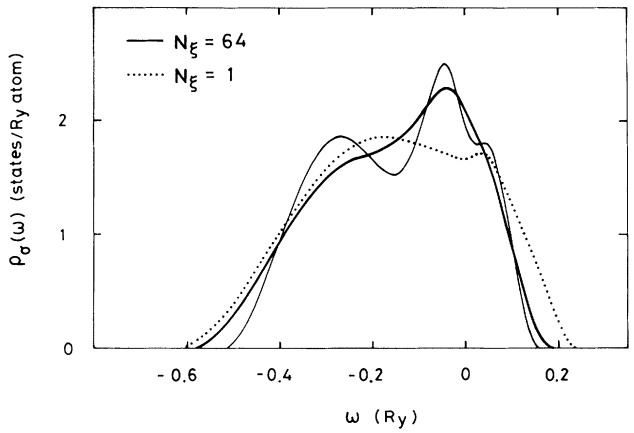

FIG. 9. Single-particle excitation spectra obtained by the numerical analytic continuation. The parameters are the same as in Fig. 8. The solid (dotted) curve denotes the dynamical case $N_\xi=64$ (the static case $N_\xi=1$) with use of the smoothing parameter $s=10^{-2}$. The dynamical results obtained with use of $s=2\times10^{-3}$ are also shown by the thin curve.

mean-squares measure with a smoothing parameter s which encourages one to smooth the curve $\rho_\sigma(\omega)$, and a positivity parameter p which encourages one to choose a positive function $\rho_\sigma(\omega)$. We have increased p, first keeping s to be a small value, until the positive spectrum is obtained, and then increased s until the spectrum for $N_\xi=1$ becomes consistent with that obtained by the analytical method.

The reconstruction of the spectra is not quantitative at present, as seen by comparing the result of $N_\xi=1$ with the analytic result in Fig. 8. This is partly due to a small number of MCS's and partly due to the difficulty in reproducing a rapid change of curve by means of the method of numerical analytic continuation used in the present calculation. The dynamical result of $N_\xi=64$ is shown in Fig. 9. The main peak for $N_\xi=64$ may be slightly overestimated because the spectrum obtained from the rectangular DOS should satisfy the inequality $\rho_\sigma(\omega)\leq 1/W$ in the single-site approximation. The present result for $N_\xi=64$ seems to show a qualitative change of the spectrum; i.e., the appearance of the shoulders due to electron and hole excitations as expected from the perturbation approach.[43]

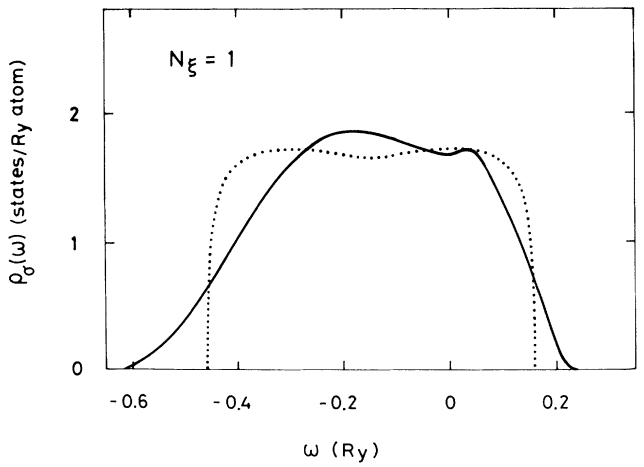

FIG. 8. Single-particle excitation spectra of the static approximation in the case of $n=1.5$, $W=0.5$ Ry, $U_0=0.2$ Ry, and $T=2000$ K. The solid curve is calculated by the numerical analytic continuation with parameter $s=10^{-2}$, while the dotted curve is calculated by the analytic theory by Hasegawa (Ref. 8).

V. SUMMARY

We have proposed the Monte Carlo dynamical CPA to go beyond the adiabatic theories in metallic magnetism. The results of numerical calculations indicate that the present approach is useful to understand the magnetism and local electron correlations at finite temperatures in the intermediate regime of the Coulomb interaction strength. We have shown in the paramagnetic state that the dynamical CPA with more than about fifty field variables along the imaginary-time axis describes the quantum effects on the amplitude of the LM. The reduction of the effective Coulomb interactions and more Fermi-liquid-like momentum distribution have also been obtained in the present approach. Calculated single-particle excitation spectra indicate that the present approach with use of $N_\xi \gtrsim 50$ field variables can describe the many-body structures as expected from the perturbation theory.

Although the Monte Carlo calculation remains qualitative or semiquantitative at present, it will be possible in the near future to improve the accuracy with use of the advanced computer algorithms and with improvements of computers. Applicability of various methods for important and fast samplings[33–36] has not yet been examined sufficiently. The use of computers with larger memory will allow for calculations at lower temperatures. Application of the maximum-entropy method[44,45] for the numerical analytic continuation of the imaginary-time Green function will lead to better single-particle excitation spectra. More systematic and accurate calculations are planned to be done in the near future, including the magnetic ordered phase.

APPENDIX A: SINGLE-PARTICLE GREEN FUNCTION IN THE SINGLE-SITE APPROXIMATION

The single-particle Green function $\mathcal{G}_{ij\sigma}(\tau-\tau')$ is given by a Green function G defined by Eq. (2.12) as follows:[46]

$$\mathcal{G}_{ij\sigma}(\tau-\tau')=\langle (G)_{i\tau j\tau'\sigma}\rangle \ . \tag{A1}$$

Here $\langle\ \rangle$ means a thermal average with respect to the energy functional $E[\xi,\eta]$ [see Eq. (2.29)].

The Green function G satisfies the following Dyson equation as derived from Eqs. (2.13) and (2.17):

$$G=\tilde{G}+\tilde{G}\delta v G \tag{A2}$$

Taking into account the submatrices that are diagonal with respect to the site, we obtain

$$G_{ii}\approx\tilde{G}_{ii}+\tilde{G}_{ii}\delta v_i G_{ii} \ . \tag{A3}$$

Thus,

$$G_{ii}=(F_i^{-1}-\delta v_i)^{-1} \ . \tag{A4}$$

Substituting Eq. (A4) into Eq. (A1) and using the CPA equation (2.29), we obtain the following relation in the single-site approximation:

$$\mathcal{G}_{ii\sigma}(\tau-\tau')=F_\sigma(\tau-\tau') \ . \tag{A5}$$

The above equation implies that the coherent potential is identical with the self-energy of the temperature Green function in the single-site approximation.

APPENDIX B: DERIVATION OF EQ. (2.34)

We derive here Eq. (2.34). Equation (2.33) is obtained in the same way. The local magnetization $\langle m_i\rangle$ is given by the formula

$$\langle m_i\rangle=-\frac{\partial\mathcal{F}_{\rm CPA}}{\partial h_i}=-\left\langle\frac{\partial E_i[\xi_i,\eta_i]}{\partial h_i}\right\rangle \ . \tag{B1}$$

Here we used the stationary condition (2.30); thus $\partial E_i/\partial h_i$ stands for taking the derivative independently of the coherent potential. We have then the identity

$$-\frac{\partial E_i[\xi_i,\eta_i]}{\partial h_i}=\sum_n\left[-\frac{2}{J_i}\frac{\partial E_i}{\partial\xi_i(\tau_n)}+\frac{\Delta\tau}{\beta}\xi_i(\tau_n)\right] \ . \tag{B2}$$

Substituting Eq. (B2) into Eq. (B1), we obtain

$$\langle m_i\rangle=-\sum_n\frac{2}{J_i}\left\langle\frac{\partial E_i}{\partial\xi_i(\tau_n)}\right\rangle+\left\langle\frac{1}{\beta}\sum_n\xi_i(\tau_n)\Delta\tau\right\rangle \ . \tag{B3}$$

The first term at the rhs of Eq. (B3) vanishes after integration by parts. Therefore, we obtain the formula (2.34).

APPENDIX C: DERIVATION OF THE AMPLITUDE OF LOCAL MOMENT (2.36)

The amplitude of the local moment is obtained from the relation $\langle m_i^2\rangle=-4\partial\mathcal{F}_{\rm CPA}/\partial J_i$. By making use of the stationary condition (2.30), we have

$$\frac{\partial\mathcal{F}_{\rm CPA}}{\partial J_i}=-\frac{1}{2}\sum_\sigma\sigma\frac{1}{\beta}\int_0^\beta d\tau\langle\xi_i(\tau)[(F_i^{-1}-\delta v_i)^{-1}]_{\tau\tau\sigma}\rangle+\frac{1}{4\beta}\int_0^\beta d\tau\langle\xi_i(\tau)^2\rangle-\frac{1}{2J_i\Delta\tau} \ . \tag{C1}$$

Here the Green function $(F_i^{-1}-\delta v_i)^{-1}$ in the first term at the rhs of Eq. (C1) appears in $\partial E_i/\partial\xi_i(\tau)$ as follows:

$$\frac{\partial E_i[\xi]}{\partial\xi(\tau)}=-\frac{1}{2}J_i\sum_\sigma\sigma\frac{\Delta\tau}{\beta}[(F_i^{-1}-\delta v_i)^{-1}]_{\tau\tau\sigma}+\frac{J_i}{2\beta}\xi_i(\tau)\Delta\tau \ . \tag{C2}$$

Thus Eq. (C1) is written as follows:

$$\frac{\partial\mathcal{F}_{\rm CPA}}{\partial J_i}=\frac{1}{J_i\Delta\tau}\int_0^\beta d\tau\left\langle\xi_i(\tau)\frac{\partial E_i}{\partial\xi_i(\tau)}\right\rangle-\frac{1}{4\beta}\int_0^\beta d\tau\langle\xi_i(\tau)^2\rangle-\frac{1}{2J_i\Delta\tau} \ . \tag{C3}$$

By integration by parts, we can verify

$$\left\langle\xi_i(\tau)\frac{\partial E_i}{\partial\xi_i(\tau)}\right\rangle=\beta^{-1} \ . \tag{C4}$$

Therefore Eq. (C3) reduces to Eq. (2.36):

$$\langle m_i^2\rangle=\frac{1}{\beta}\int_0^\beta d\tau\langle\xi_i(\tau)^2\rangle-\frac{2}{J_i\Delta\tau} \ . \tag{C5}$$

Equation (2.35) is obtained in the same way.

[1] *Metallic Magnetism*, edited by H. Capellmann, Topics in Current Physics Vol. 42 (Springer-Verlag, Berlin, 1987); *Magnetism of Metals and Alloys*, edited by M. Cyrot (North-Holland, Amsterdam, 1982).

[2] R. L. Stratonovich, Dokl. Akad. Nauk. SSSR **115**, 1097 (1958) [Sov. Phys.—Dokl. **2**, 416 (1958)].

[3] J. Hubbard, Phys. Rev. Lett. **3**, 77 (1959).

[4] M. Cyrot, J. Phys. (Paris) **33**, 25 (1972).

[5] M. C. Gutzwiller, Phys. Rev. Lett. **10**, 159 (1963).

[6] J. Hubbard, Proc. R. Soc. London **A276**, 238 (1963).

[7] J. Hubbard, Phys. Rev. B **19**, 2626 (1979); **20**, 4584 (1979); **23**, 597 (1981).

[8] H. Hasegawa, J. Phys. Soc. Jpn. **46**, 1504 (1979); **49**, 178 (1980).

[9] P. Soven, Phys. Rev. **156**, 809 (1967); H. Ehrenreich and L. M. Schwarz, *Solid State Physics*, edited by H. Ehrenreich, F. Seitz, and D. Turnbull (Academic, New York, 1980), Vol. 30.

[10] H. Hasegawa, J. Phys. Soc. Jpn. **49**, 963 (1980); J. Phys. F **13**, 1915 (1983); N. Evangelou and D. M. Edwards, J. Phys. C **16**, 2121 (1983); H. Hasegawa and D. G. Pettifor, Phys. Rev. Lett. **50**, 2251 (1981).

[11] Y. Kakehashi, J. Phys. Soc. Jpn. **50**, 2251 (1981); Phys. Rev. B **34**, 3243 (1986).

[12] Y. Kakehashi, J. Phys. Soc. Jpn. **46**, 2421 (1980); **50**, 2236 (1981); Prog. Theor. Phys. Suppl. **101**, 105 (1990).

[13]H. Hasegawa, J. Phys. Soc. Jpn. **50**, 802 (1981).
[14]H. Hasegawa, J. Phys. F **16**, 347 (1986); **16**, 1555 (1986); **17**, 165 (1987); Surf. Sci. **182**, 591 (1987).
[15]Y. Kakehashi, Phys. Rev. B **40**, 11 063 (1989).
[16]Y. Kakehashi, Phys. Rev. B **41**, 9207 (1990); **43**, 10 820 (1991).
[17]T. Oguchi, K. Terakura, and N. Hamada, J. Phys. F **13**, 761 (1983); B. L. Gyorffy, A. J. Pinder, J. S. Staunton, G. M. Stocks, and H. Winter, *ibid.* **15**, 1337 (1985).
[18]T. Moriya and H. Hasegawa, J. Phys. Soc. Jpn. **48**, 1490 (1980).
[19]H. Hasegawa, Solid State Commun. **38**, 401 (1981).
[20]Y. Kakehashi, J. Phys. Soc. Jpn. **50**, 1505 (1981).
[21]J. H. Samson, J. Phys. (Paris) **45**, 1675 (1984); Y. Kakehashi, Phys. Rev. B **31**, 3104 (1985).
[22]J. Kanamori, Prog. Theor. Phys. **30**, 235 (1963); J. A. Hertz and D. M. Edwards, J. Phys. F **3**, 2174 (1973).
[23]Y. Kakehashi and P. Fulde, Phys. Rev. B **32**, 1595 (1985).
[24]Y. Kakehashi, Phys. Rev. B **38**, 6928 (1988).
[25]G. Stollhoff and P. Fulde, Z. Phys. B **29**, 231 (1978); J. Chem. Phys. **73**, 4548 (1980); A. M. Oleś and G. Stollhoff, Phys. Rev. B **29**, 314 (1984).
[26]Y. Kakehashi and J. H. Samson, Phys. Rev. B **34**, 1734 (1986); Y. Kakehashi, Physica B **161**, 143 (1989).
[27]H. Hasegawa, J. Phys. Condensed Matter **1**, 9325 (1990).
[28]G. Kotliar and A. E. Ruckenstein, Phys. Rev. Lett. **57**, 1362 (1986).
[29]E. A. Turov and V. I. Grebenikov, Physica B **149**, 150 (1988).
[30]S. Hirooka and M. Shimizu, J. Phys. Soc. Jpn. **43**, 70 (1977).
[31]J. A. Hertz and M. A. Klenin, Phys. Rev. B **10**, 1084 (1974); Physica B&C **91B**, 49 (1977).
[32]For a recent review on the Monte Carlo method, see *Application of the Monte Carlo Method in Statistical Physics,* edited by K. Binder (Springer, Berlin, 1984); M. H. Kalos and P. A. Whitlock, *Monte Carlo Methods* (Wiley, New York, 1986); *Quantum Monte Carlo Methods,* edited by M. Suzuki (Springer, Berlin, 1984).
[33]R. Blankenbecler, D. T. Scalapino, and R. L. Sugar, Phys. Rev. D **24**, 2278 (1981).
[34]J. E. Hirsch, Phys. Rev. B **31**, 4403 (1985).
[35]R. T. Scaletter, D. J. Scalapino, R. L. Sugar, and D. Toussaint, Phys. Rev. B **36**, 8632 (1987).
[36]J. E. Hirsch, Phys. Rev. B **35**, 1851 (1987).
[37]Y. Kakehashi and H. Hasegawa, Phys. Rev. B **36**, 4066 (1987); **37**, 7777 (1988).
[38]R. T. Scaletter, D. J. Scalapino, R. L. Sugar, and D. Toussaint, Phys. Rev. B **39**, 4711 (1989).
[39]For a recent review on heavy fermions see P. Fulde, J. Keller, and G. Zwicknagl, Solid State Phys. **41**, 1 (1988).
[40]S. Q. Wang, W. E. Evenson, and J. R. Schrieffer, Phys. Rev. Lett. **23**, 92 (1969); J. Appl. Phys. **41**, 1199 (1970).
[41]M. Sakoh and M. Shimizu, J. Phys. Soc. Jpn. **40**, 974 (1976).
[42]S. R. White, D. J. Scalapino, R. L. Sugar, and N. E. Bickers, Phys. Rev. Lett. **63**, 1523 (1989).
[43]G. Treglia, F. Ducastelle, and D. Spanjaard, J. Phys. (Paris) **41**, 281 (1980).
[44]S. F. Gull and J. Skilling, IEEE Proc. **131**(F), 646 (1984).
[45]R. N. Silver, D. S. Sivia, and J. E. Gubernatis, Phys. Rev. B **41**, 2380 (1990); R. N. Silver, J. E. Gubernatis, D. S. Sivia, and M. Jarrel, Phys. Rev. Lett. **65**, 496 (1990).
[46]D. R. Hamann, Phys. Rev. B **2**, 1373 (1970).